Journal of Optoelectronics and Advanced Materials Vol. 7, No. 1, February 2005, p. 73 - 81

Invited Paper

ELECTRONIC PROPERTIES OF HYDROGENATED AMORPHOUS SILICON PREPARED IN EXPANDING THERMAL PLASMAS

M. Brinza*, G. J. Adriaenssens

Laboratorium voor Halfgeleiderfysica, University of Leuven, Celestijnenlaan 200D, B-3001 Leuven, Belgium

The expanding thermal plasma (ETP) technique allows the deposition of hydrogenated amorphous silicon (a-Si:H) layers at rates up to 10 nm/s. Schottky barrier cells from Eindhoven University of Technology and p-i-n structures from Delft University of Technology have been examined with the time-of-flight transient photoconductivity technique to determine the carrier mobilities, tail state distributions and gap state densities of the material in function of the deposition parameters. To obtain electronic-quality material at high deposition rates, it is necessary to use substrate temperatures as high as 450 °C. As a function of the chosen deposition parameters, ETP a-Si:H does reveal a wide spectrum of electronic properties, ranging from characteristics close to those of a-Si:H made by standard plasma-enhanced chemical vapour deposition, to evidence for nanoscopic ordered inclusions of the type found in so-called polymorphous silicon layers. One hallmark property of the best ETP a-Si:H is a remarkably high hole drift mobility of ~10^{-2} cm^2 $V^{-1}s^{-1}$. Gap state densities of 10^{16} cm^{-3} eV^{-1} and above have been measured.

(Received December 9, 2004; accepted January 26, 2005)

Keywords: Hydrogenated amorphous silicon, Plasma deposition, Drift mobility, Time-of-flight photocurrents, Nanostructure

1. Introduction

Since amorphous silicon solar cells, which represent a significant part of the practical interest in hydrogenated amorphous silicon (a-Si:H), have to operate in an area where reduction of production cost remains an important factor, there is a continuing interest not only in improving the material quality and finding an answer to the efficiency-reducing Staebler-Wronski effect, but also in increasing the throughput in the deposition stage of the a-Si:H layers. One technique that is able to realise a high a-Si:H deposition rate is the Expanding Thermal Plasma (ETP) method that was initiated at the Eindhoven University of Technology [1-3]. It is a remote plasma technique whereby the film growth from pure SiH_4 is realised some distance away from the Ar + H_2 plasma source, and deposition rates of up to 10 nm/s can be achieved. Depositions have been carried out under varying circumstances of – primarily – gas flow rate and substrate temperature, with ellipsometry available as in-situ diagnostic tool and a systematic post-deposition infrared absorption test carried out to ensure consistent material quality. In the following sections, investigations into the electronic properties of the ETP a-Si:H layers will be summarised, with mayor emphasis on the results of electron and hole drift mobility measurements and on the density of localised states in the a-Si:H band gap as determined from time-of-flight (TOF) photoconductivity experiments [4]. It should be noted that results of earlier transient photocurrent measurements on ETP samples, as published in previous reports [5,6], are confirmed by the present more comprehensive investigation as far as the drift mobility data are concerned, but that our initial interpretation of the final part of the current

* Corresponding author: monica.brinza@fys.kuleuven.ac.be

transient in terms of the gap-state density was mistaken, and has since been revised [7,8]. Results from other experimental techniques, where available, will be compared to the ones derived from the TOF data.

2. Experimental details

ETP a-Si:H samples are currently being prepared at two Dutch Universities: the Eindhoven University of Technology where the technique originated, and the DIMES Laboratory of the Delft University of Technology where solar cells with an ETP a-Si:H intrinsic layer are being investigated. a-Si:H samples from both Universities, but no actual solar cells have been included in the research reported here.

2.1 Characteristics of ETP a-Si:H samples

Since time-of-flight transient photocurrent spectroscopy (outlined below), being the principal experimental technique used in the present study, requires a-Si:H layers of several micrometer thick for measurements of the electron drift mobility near room temperature, most of our samples are based on such uncommonly thick layers. Unfortunately, some of the thicker films did peel off the substrate after a few cycles of heating and cooling. TOF samples from Eindhoven were generally deposited at rates of 5 to 7 nm/s on Cr-covered glass substrates to thicknesses of 2.4 to 7.7 µm. Substrate temperatures ranged from 250 to 500 °C. Small circular semi-transparent Cr top contacts were subsequently sputtered on to establish Schottky barrier sandwich cells. For one 400 °C cell, Cr was replaced by Mo. At Delft, samples were prepared at either 2nm/s and 400 °C or 0.85 nm/s and 250 °C in the form of both Cr- and Mo-based Schottky diodes and as p^+-i-n^+ structures, all with layer thicknesses of both 2.9 to 3.6 µm and ~5.5 µm.

Separate sample series (with no pre-deposited electrical contacts) were prepared for material characterisation by photothermal deflection spectroscopy (PDS), constant photocurrent method (CPM) or X-ray photoelectron and emission spectroscopy (XPS, XES). These layers were ~1 µm thick, deposited at some 2 or 8 nm/s for a range of substrate temperatures from 200 to 500 °C, on either Corning 7059 glass or (for the X-ray spectroscopy) thin steel substrates.

2.2 Time-of-flight transient photocurrent technique

For TOF experiments electron-hole pairs are generated through the semi-transparent electrode of the sandwich cell by means of a short, strongly absorbed laser pulse. Shortly before the light pulse is triggered, an electric field is applied across the sample such that – depending on the polarity of the field or the orientation of the p-i-n cell – photo-generated electrons or holes will drift through the sample. A primary photocurrent will be measured in an external circuit due to the charge displacement in the sample, but secondary photocurrents will be blocked by the potential barriers at the interfaces. The transit time through the cell of the mean of the generated carrier distribution, t_T, can be deduced from a drop in the primary photocurrent; it allows calculation of the carrier drift mobility, provided the electric field remained uniform during the transit. Details of the experimental TOF set-up may be found in earlier reports [5,9].

2.3 Other characterisation techniques

The electronic structure of selected sample series was further examined by means of photoluminescence (PL) at 77 K to study the defect structure, by the constant photocurrent method as well as by photothermal deflection spectroscopy to probe the sub-band-gap absorption, and through the use of X-ray photoelectron and X-ray emission spectroscopies to explore the valence band edge. PL and CPM measurements were carried out in our laboratory, PDS data were obtained from the Institute of Materials Research (Diepenbeek, Belgium) and X-ray spectroscopy was done in collaboration with the Laboratoire de Chimie Physique (Paris, France). The essential results and details of the experimental arrangements may be found in recent reports [10,11].

3. Carrier drift mobilities

With the TOF experiment, the hole or electron drift mobility is determined on the basis of the measured carrier transit time t_T by means of the equation $\mu_d = L/t_T F$, where L is the layer thickness and F the applied electric field. Drift mobility data sets as a function of sample thickness, temperature and applied field can be used to model the tail-state distributions (see next section). Fig. 1 shows representative sets of hole and electron drift mobility data from ETP a-Si:H samples of varying thickness, prepared at high deposition rate and different substrate temperatures. The hole mobilities show a very regular pattern, with the position of an individual sample in the pattern determined by the substrate temperature at deposition. The 3 straight lines represent samples deposited at (top to bottom) 450, 400 and 250 °C. The 1.1×10^{-2} cm^2 V^{-1} s^{-1} room temperature hole mobility of the 450 °C sample represents the highest confirmed hole mobility measured to date [12]. The individual symbols on the middle solid line represent 3 different *L* and 4 different *F* values; the hole mobility is obviously not sensitive to these parameters. This observation remains valid for all depositions that were carried out at high growth rate or at high substrate temperature. For sample depositions at low growth rate (0.85 nm/s) and low temperature (250 °C), a field dependence of the mobility is observed. One such case is discussed in the next section.

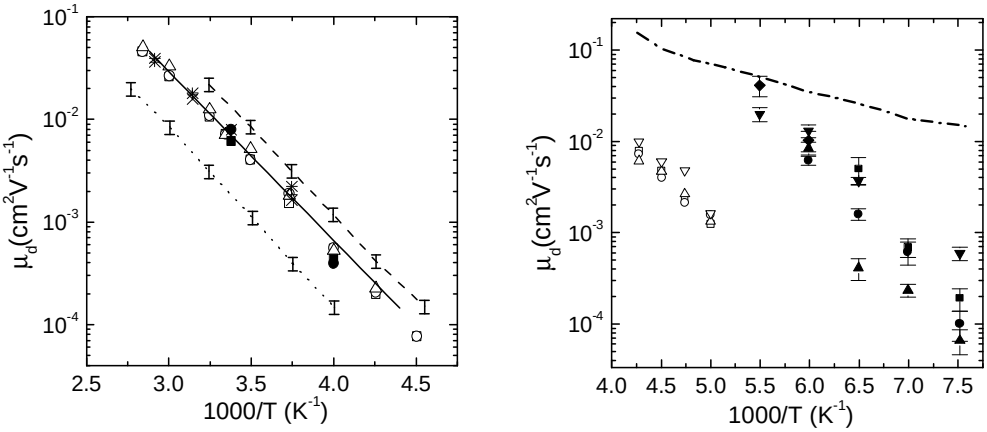

Fig. 1. Temperature dependence of the hole drift mobility (left) and electron drift mobility (right) in ETP a-Si:H samples deposited at ~ 6 nm/s for substrate temperatures of 250, 400 and 450 °C. Sample thickness varied from 2 to 6 μm, and applied fields from 3 to 27 kV/cm. Further details may be found in [6].

The electron mobility, in contrast to the hole mobility, does not show a regular pattern. Depending on individual samples, the temperature dependence of the mobility can be weak or strong as seen in the right-hand panel of Fig. 1. Most samples were too thin to measure the electron transit time at room temperature, but from the few available data for that parameter it may be concluded that $\mu_e \cong 1$ cm^2 V^{-1} s^{-1} for the better samples.

In an attempt to understand the reason for the unexpectedly high hole mobility, the electronic structure of the ETP a-Si:H valence band tail was compared through XPS and XES to the one of a standard PECVD (plasma-enhanced chemical vapour deposition) sample [10]. No significant differences could be observed in either the overall distribution of states given by XPS, or in the p component of the bonding orbitals as measured by Si Kβ XES. The Si $L_{II,III}$ spectra on the other hand do show a small difference in the s character of the valence band wavefunctions between ETP and PECVD samples. A lobe of the s spectrum that protrudes in the band gap is more outspoken in the ETP material. One may speculate that this increased density of the less localised orbital could facilitate hopping conduction of the holes.

4. Distribution of tail states

TOF spectroscopy has been the primary method for establishing the exponential character of the a-Si:H tail state distributions [13]. Unlike techniques that measure a convolution of valence and conduction band tails, TOF can examine electron an hole transport separately. The dispersive nature of the multiple-trapping carrier transport in amorphous semiconductors, and in a-Si:H in particular, creates a time- and electric-field-dependent carrier mobility wherefrom the distribution of localised states that supports that transport can be extracted in principle [14]. In practice however, TOF data have mostly been compared to the predictions for an exponential distribution $g(E) = g(0)\exp(-E/E_0)$ only. Two methods have been used: From the pre-transit slope of the current transient, $I(t) \propto t^{-(1-\alpha)}$, the parameter $\alpha = kT/E_0$ is extracted and the width E_0 of the exponential tail calculated, or one obtains α from the relationship

$$\mu_d \propto (L/F)^{-(1-1/\alpha)} \tag{1}$$

predicted for the drift mobility in case of an the exponential tail state distribution.

An example of the latter method is shown in Fig. 2. It relates to hole transients in ETP samples deposited at 0.85 nm/s and with 250 °C as substrate temperature. The μ_d versus L/F curves do allow for the determination of the α values displayed in Fig. 2(b). If the valence band tail would be strictly exponential, $\alpha = kT/E_0$ would be found and the full line through the α values would also pass through the origin. That is clearly not the case here, but an approximating exponential of width kT_c = 37 meV can be resolved by connecting the average value of α to the origin. (This is actually the 'established' procedure that has been used since the early Tiedje *et al.* papers [15].) Estimates for the valence band tail width on the basis of the $t^{-(1-\alpha)}$ power law of the pre-transit current do give similar values. This 37 meV width is lower than the accepted value of ~45 meV for standard PECVD a-Si:H. For the width of the ETP a-Si:H conduction band tail, the pre-transit slope indicates values near 33 meV, which is considerably larger than the 22 to 26 meV generally quoted for PECVD samples. Better determinations of the tail state distributions can be achieved in the multiple-trapping formalism by fitting the current transients to a more general analytic expression for the DOS than the pure exponential one, as will be discussed in section 6.

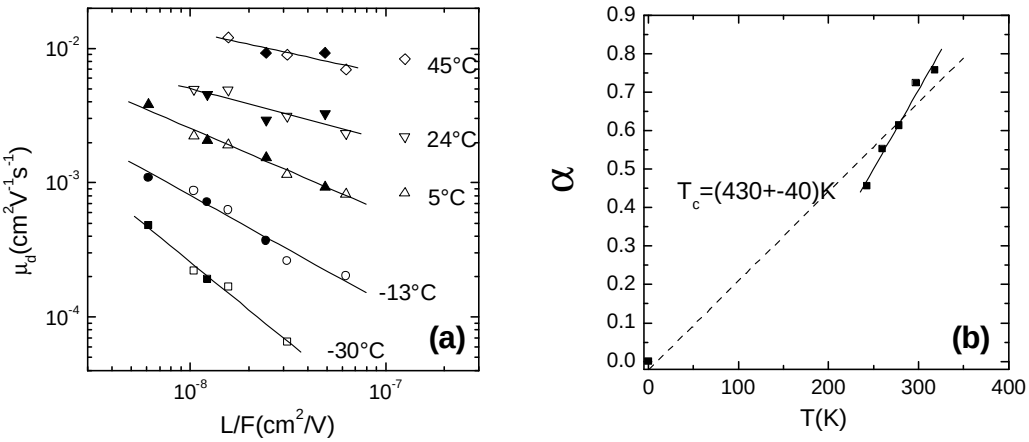

Fig. 2. (a) Dependence of the hole drift mobility on *L/F* at the indicated temperatures for 3.5 µm (solids symbols) and 5.6 µm (open symbols) thick samples prepared at 0.85 nm/s onto substrates held at 250 °C; (b) Values of α extracted from the data in (a).

5. Distribution of gap states

Photo-excited carriers will be trapped not just in the band tails but also deeper in the gap of the semiconductor. Given that the release probability of a trapped carrier decreases exponentially

with the trap depth, deeply trapped carriers will only contribute to the signal in a transient photocurrent experiment at long times. In the TOF experiment, it is the post-transit current at times $t >> t_T$ that will contain the gap state information. It was shown [16] that, under conditions of equal capture probability and no deep retrapping, the DOS can be calculated from $I(t)$ according to

$$g(E) = \frac{2g(0)}{Q_0 t_0 \nu} I(t) \cdot t \quad , \quad E = kT \ln(\nu t) \ , \tag{2}$$

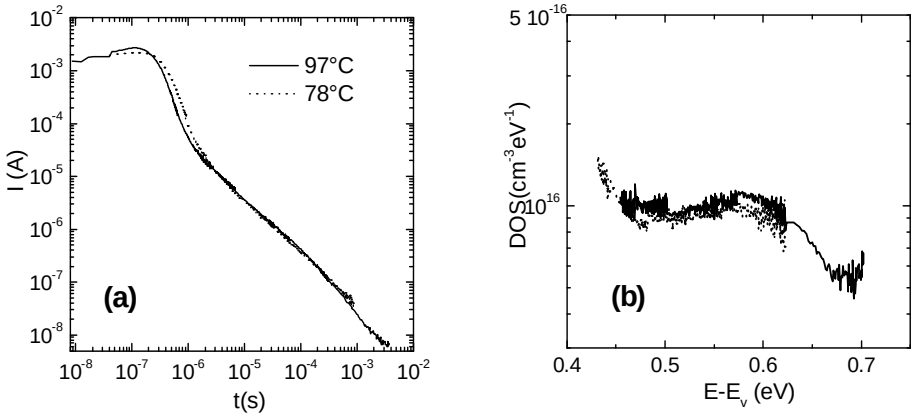

Fig. 3. (a) TOF hole transients, showing the post-transit regime, from a 2 µm sample deposited at 6 nm/s and 450°C, and with 10 V applied; (b) DOS profile calculated from them with Eq. (2), $Q_0 = 2 \times 10^{-9}$ C, $\nu = 10^{12} s^{-1}$, $g(0) = 10^{21}$ cm^{-3}eV^{-1} and $\mu_0 = 8$ cm^{2}V^{-1}s^{-1}.

where Q_0 is the total charge in the transient, t_0 is the free carrier transit time, ν the attempt-to-escape frequency, and g(0) is the DOS at the mobility edge. It should be noted that Q_0 and ν can be estimated on the basis of a set of TOF transients, but that the parameters g(0) and t_0 have to be obtained from elsewhere. Fig. 3 shows an example. The choice of those parameters does, of course, directly influence the calculated values of the gap state density. For the various series of ETP a-Si:H samples that were examined, gap state densities have been found from just below 10^{16} cm^{-3}eV^{-1} for the better samples to several times that value for the poorer ones.

After the initial studies of the post-transit currents [5,6], it was discovered that part of the measured current was not related to charge emission from deep traps, but rather a consequence of photoinduced barrier lowering at the illuminated Cr/a-Si:H interface. Previously reported gap state densities were, therefore, amended in [8] to the values cited above. Similar problems were not encountered when Mo was used for the Schottky contact, or with the p-i-n structures, nor for that matter when Cr is used on PECVD a-Si:H. The reason behind the specific behaviour of the Cr/(ETP a-Si:H) contact has not been discovered.

The gap state densities have also been evaluated on the basis of the more traditional CPM and PDS techniques. Results from CPM measurements on 1 µm thick films deposited at 8 and 2 nm/s for several substrate temperatures are shown in Fig. 4. The lowest gap-state absorption is clearly obtained with the more slowly deposited samples. Using the conventional conversion factor between absorption coefficient and density of states [11], the 2nm/s samples do have gap state densities of 2 to 7×10^{16} cm^{-3}eV^{-1}, in line with the values obtained from the post-transit analysis. The results from the 8nm/s depositions on the other hand indicate densities above 5×10^{16} cm^{-3}eV^{-1}, considerably higher than measured for the films deposited at 6 nm/s that were examined by TOF. In general, higher deposition rates do result in higher defect densities.

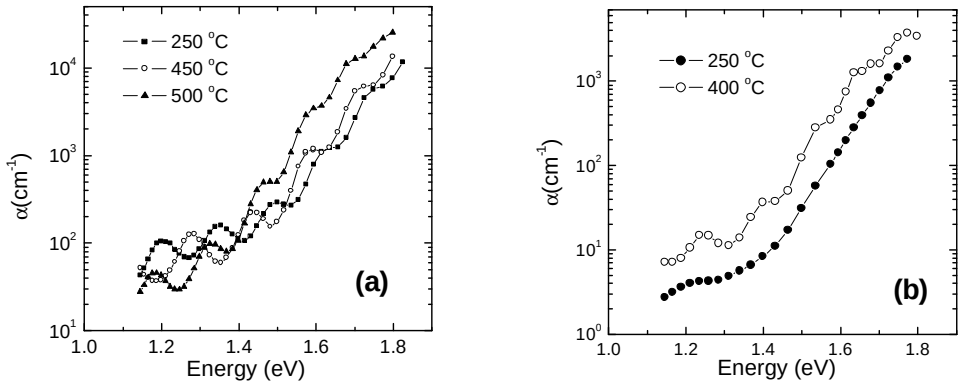

Fig. 4. Energy dependence of the optical absorption coefficient α as derived from CPM measurements on 1 μm thick ETP a-Si:H layers deposited at the indicated temperatures [11]; (a) samples deposited at 8 nm/s; (b) samples deposited at 2 nm/s.

6. Evidence for nanostructure

Photoluminescence characterisation of several ETP a-Si:H layers prepared under different conditions showed radiative transitions in the range of 1.2 to 1.3 eV, always well short of the expected 1.4 eV transition of a-Si:H. Since such lower PL energies have been reported for a-Si:H samples with increased disorder through the presence of either microcrystals [17] or voids [18], the possibility that similar disruptions of the amorphous lattice might occur in the ETP a-Si:H samples was investigated. In fact, Smets [19] already reported a narrowing of the X-ray diffraction line that might indicate some structural ordering in the layer, Kessels *et al.* [20] observed hydrogen-poor cationic clusters in the growth plasma, and recently Smets *et al.* [21] described the occurrence of divacancies and voids in some ETP layers.

Support for the presence of structured inhomogeneities in the amorphous matrix of ETP a-Si:H layers, or at least in those deposited at 2 nm/s or faster, is provided by an analysis of the TOF current transients. As mentioned above, the hole drift mobility is field independent for the samples deposited at a high rate, and the electron mobility is very unpredictable. We believe that both phenomena can be explained by the presence of a distribution of crystal-like inclusions in the amorphous material.

The field-independent drift mobility signifies that the photoinduced carrier distribution has reached a virtual equilibrium by the time the mean of that distribution reaches the back electrode of the TOF sample. As discussed in detail in a separate contribution [22], equilibrium behaviour can never occur in a purely exponential distribution of tail states. Only in a more steeply declining distribution of states can equilibrium be established. Consequently, to model the TOF current transients, the DOS has to include more than just exponentially varying components. A Gaussian component in the DOS would satisfy the 'steeper-decline' requirement and would also fit in with the assumption of a random distribution of lattice perturbing inclusions.

Calculations of the current transients were carried out on the basis of the analytic multiple-trapping transport equations derived for the TOF experiment by Arkhipov and Rudenko [23]. In the procedure, theoretical pre- and post-transit-time currents are calculated and joined into a continuous curve at the transit time, the latter being defined by the time the mean of the carrier distribution needs to travel the sample distance L. The input to the calculations consists of the density of states function $g(E)$, the experimental values for L, F, T and Q_0, and best estimates for the constants involved, *i.e.* the effective state density at the mobility edge N_C, the free-carrier mobility μ_0 and the attempt frequency ν [9,22]. It is crucial for a good result to have access to an experimental data set with sufficient variation in the measurement parameters. Measurements at various fields but for just one temperature may fit well to a DOS function that proves totally inadequate when used for transients measured at a different temperature on the same sample. An example of a successful

fitting can be seen in Fig. 5, where data obtained with 3 different fields at 3 different temperatures are shown. The density of states used for the fits of Fig. 5 was of the form

$$g(E) = \frac{N_{tE}}{E_0}\exp\left(\frac{-E}{E_0}\right) + \left(\frac{2}{\pi}\right)^{1/2}\frac{N_{tG}}{\sigma}\exp\left(\frac{-(E-E_G)^2}{2\sigma^2}\right), \quad (3)$$

with $N_{tE} = 6 \times 10^{18}$ cm^{-3}, $E_0 = 40$ meV, $N_{tG} = 2.5 \times 10^{19}$ cm^{-3}, $\sigma = 87$ meV, and $E_G = 60$ meV. It is the Gaussian component of Eq. (3) that is dominant and thus allows field independence of the drift mobility to be duplicated in the calculations. Similar results apply to all but the 0.85 nm/s ETP samples. With the latter ones, the exponential component dominates.

The prominent Gaussian DOS component, having its maximum inside the amorphous gap, can be seen as evidence for the presence of differently structured inclusions in the ETP a-Si:H samples. Indeed, the internal interfaces between the a-Si:H and the inclusions would contain a distribution of weaker Si-Si bonds and could thus generate the observed Gaussian component. Should the random inclusions be crystalline in nature, then their upper valence band states would act as traps inside the amorphous gap and contribute to the Gaussian component. More speculative is our suggestion that the postulated nanoscale inclusions can also explain the observed unpredictability of the electron mobility in our samples. It does require that the inclusions be quasi-crystalline. With the crystalline band gap being smaller than the amorphous one, quantum confinement in individual grains of varying size will generate a (normal) distribution of widened crystalline gaps. Since it has been established [24] that band offsets between the amorphous and crystalline phases are situated mainly at the valence band side, it follows that the small conduction band offset between the amorphous matrix and the inclusions may very well depend on preparation conditions and thus differ somewhat, or even change sign, between samples. Electron transport would then be influenced by these varying conditions in individual samples, while small variations in the larger offset at the valence band side, would have little influence on the hole mobility.

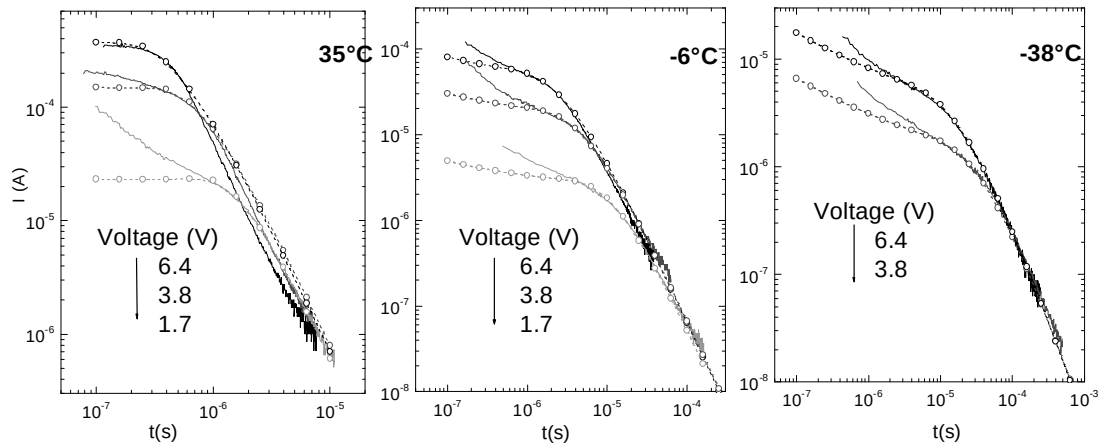

Fig. 5. Comparison between measured (full lines) and calculated (symbols and dashes) TOF hole transient currents from a 2.4 μm thick sample, deposited at 5.6 nm/s and 450 °C, and measured with Cr Schottky contacts. For details of the calculations: see text.

7. Concluding remarks

The aim of the ETP project is the production of solar-cell quality a-Si:H at high deposition rates. From the results outlined in the previous sections it follows that a-Si:H of acceptable quality can be deposited for the moment at rates as high as 6 to 7 nm/s, provided that the substrate temperature is kept near 450 °C. Further adjustment to experimental procedures and parameters

may still be able to improve material properties, but the requirement of a high deposition temperature precludes the application of such material for solar cell purposes. At lower temperatures, good material quality is only obtained with lower deposition rates. Samples prepared at 250 °C and 0.85 nm/s are actually rather similar to standard PECVD samples.

The nanostructure that has been observed in the ETP a-Si:H layers is reminiscent of the structured inclusions in polymorphous silicon [25]. In fact, the cited observation of hydrogen-poor cationic clusters in the ETP-a-Si:H growing plasma [20] may indicate the influence of comparable processes. As with polymorphous silicon, the presence of ordered inclusions may bring about some improved transport properties, *e.g.*, the high hole mobility in ETP a-Si:H.

The measured distribution of localised states in the band gap of ETP a-Si:H deviates to some extent from the pattern set by PECVD a-Si:H. A somewhat steeper valence band tail and a somewhat less steep conduction band tail is resolved, together with a generally higher density of gap states. More data that specifically aim at the tail state distributions will be required to see whether this is an intrinsic characteristic of the ETP material or just a coincidental result of the current set of measurements.

In summary, we may conclude that deposition rates of a-Si:H as high as 10 nm/s can be reached by allowing an expanding thermal plasma of Ar and H_2 to decompose the injected SiH_4 gas. However, there is an unfavorable link between deposition rate and deposition temperature for achieving good material quality, with the desired high deposition rates only producing low-quality films at low substrate temperatures for the moment.

Acknowledgments

The authors owe special thanks to Arno Smets and Agnès Petit for preparing the series of ETP a-Si:H samples, to Erwin Kessels and Richard van de Sanden for useful discussions about the ETP material, and to Zhenja Emelianova and Vladimir Arkhipov for help with the multiple-trapping analyses. We also are grateful to Jan Willekens for the CPM measurements, to Kostya Iakoubovskii for the PL results, to Esther Belin-Ferré and Adriana Gheorghiu-de La Rocque for their help with the X-ray spectroscopy, and to the *Fonds voor Wetenschappelijk Onderzoek - Vlaanderen* for financial support of this research.

References

[1] M. C. M. van de Sanden, R. J. Severens, W. M. M. Kessels, R. F. G. Meulenbroeks, D. C. Schram, J. Appl. Phys. **84**, 2426 (1998).
[2] W. M. M. Kessels, R. J. Severens, M. C. M. van de Sanden, D. C. Schram, J. Non-Cryst. Solids **227**, 133 (1998).
[3] W. M. M. Kessels, C. M. Leewis, M. C. M. van de Sanden, D. C. Schram, J. Appl. Phys. **86**, 4029 (1999).
[4] M. Brinza, Carrier mobility and density of states in hydrogenated amorphous silicon prepared in expanding thermal plasmas, Ph. D. thesis, K. U. Leuven (2004).
[5] G. J. Adriaenssens, H.-Z. Song, V. I. Arkhipov, E. V. Emelianova, W. M. M. Kessels, A. H. M. Smets, B. A. Korevaar, M. C. M. van de Sanden, J. Optoelectron. Adv. Mater. **2**, 31 (2000).
[6] M. Brinza, G. J. Adriaenssens, K. Iakoubovskii, A. Stesmans, W. M. M. Kessels, A. H. M. Smets, M. C. M. van de Sanden, J. Non-Cryst. Solids **299**, 420 (2002).
[7] M. Brinza, G. J. Adriaenssens, J. Mater. Sci.: Mater. Electron. **14**, 749 (2003).
[8] M. Brinza, W. M. M.Kessels, A. H. M.Smets, M. C. M.van de Sanden, G. J. Adriaenssens, Mater. Res. Soc. Symp. Proc. **762**, 99 (2003).
[9] M. Brinza, E. V. Emelianova, A. Stesmans, G. J. Adriaenssens, Mater. Res. Soc. Symp. Proc. **808**, A5.6 (2004).
[10] E. Belin-Ferré, A. Gheorghiu-de La Rocque, M.-F. Fontaine, J. Thirion, M.Brinza, J. Willekens, G. J. Adriaenssens, J. Non-Cryst. Solids **338**, 240 (2004).
[11] J. Willekens, M. Brinza, T. Güngör, G. J. Adriaenssens, M. Nesládek, W. M. M. Kessels, A. H. M. Smets, M. C. M. van de Sanden, J. Non-Cryst. Solids **338**, 244 (2004).

[12] S. Dinca, G. Ganguly, Z. Lu, E. A. Schiff, V. Vlahos, C. R. Wronski, Q. Yuan, Mater. Res. Soc. Symp. Proc. **762**, 345 (2003).
[13] R. A. Street, Hydrogenated amorphous silicon, Cambridge University Press, Cambridge, U.K. (1991).
[14] J. M. Marshall, Rep. Prog. Phys. **46**, 1235 (1983).
[15] T. Tiedje, J. M. Cebulka, D. L. Morel, B. Abeles, Phys. Rev. Lett. **46**, 1425 (1981).
[16] G. F. Seynhaeve, R. P. Barclay, G. J. Adriaenssens, J. M. Marshall, Phys. Rev. B **39**, 10196 (1989).
[17] G. Yue, D. Han, D. L. Williamson, J. Yang, K. Lord, S. Guha, Appl. Phys. Lett. **77**, 3185 (2000).
[18] D. Han, G. Yue, K. Wang, J. Baugh, Y. Wu, Y. Xu, Q. Wang, Appl. Phys. Lett. **80**, 40 (2002).
[19] A. H. M. Smets, Ph. D. thesis, Eindhoven University of Technology (2002).
[20] W. M. M. Kessels, M. C. M. van de Sanden, D. C. Schram, Appl. Phys. Lett. **72**, 2397 (1998).
[21] A. H. M. Smets, W. M. M. Kessels, M. C. M. van de Sanden, Appl. Phys. Lett. **82**, 1547 (2003).
[22] E. V. Emelianova, M. Brinza, V. I. Arkhipov, G. J. Adriaenssens, ISCMP2004, these proceedings.
[23] V. I. Arkhipov, A. I. Rudenko, Philos. Mag. B **45**, 189 & 209 (1982).
[24] J. M. Essick, J. D. Cohen, Appl. Phys. Lett. **55**, 1232 (1989); J. M. Essick, Z. Nobel, Y.-M. Li, M. S. Bennett, Phys. Rev. B **54**, 4885 (1996).
[25] P. Roca i Cabarrocas, J. Non-Cryst. Solids **266**, 31 (2000).